FISEVIER

Contents lists available at ScienceDirect

International Journal of Heat and Fluid Flow

journal homepage: www.elsevier.com/locate/ijhff





Heat transfer analysis of molten salt nitrates inside shell and tube heat exchanger with small round holed segmental baffles for concentrated solar power

M.A. Khaliquzzama ^{a,*}, S.U. Masuri ^{a,b}, R. Saidur ^{c,d}, Abdul Aziz Hairuddin ^a, Suraya Mohd Tahir ^{a,b}, Norhazwani Abd Malek ^{a,e,f}

- ^a Department of Mechanical and Manufacturing Engineering, Universiti Putra Malaysia, 43400 Serdang, Selangor, Malaysia
- ^b Advanced Structural Integrity and Thermofluid Engineering (AdSITE) Research Group, Faculty of Engineering. Universiti Putra Malaysia, 43400 Serdang, Selangor, Malaysia
- ^c Research Centre for Nano-Materials and Energy Technology (RCNMET), Faculty of Engineering and Technology, Sunway University, Bandar Sunway, Petaling Jaya 47500, Malaysia
- d School of Engineering, Lancaster University, Lancaster LA1 4YW, UK
- ^e Department of Mechanical Engineering, College of Engineering, Universiti Tenaga Nasional, 43000 Kajang, Selangor, Malaysia

ARTICLE INFO

Keywords: Concentrated Solar Power (CSP) Molten salts Heat transfer performance Pressure drop reduction Thermal efficiency improvement

ABSTRACT

Investigating the heat transfer performance of molten salts for concentrated solar power (CSP) systems has posed significant challenges due to their high melting points, hence resulting in scarcity of such data. Additionally, high-pressure drops represent critical issues that need to be addressed. Conventional baffle designs contribute to these issues by causing excessive flow resistance while attempting to enhance heat transfer. Therefore, there is a need for an improved heat exchanger design that minimizes pressure drop while balancing the effective heat transfer performance. This study addresses these challenges by proposing a modified shell-and-tube heat exchanger (STHE) equipped with a novel baffle configuration featuring small round holes to enhance heat transfer efficiency and reduce pressure drop. A STHE was successfully modelled using ANSYS software for shellside analysis, adhering to Tubular Exchanger Manufacturers Association (TEMA) standards which is widely used in industries. The model was validated through comparison with previously verified experimental data and CFD modelling. Three molten salts, namely Solar Salt, Hitec, and NaKCaNO3, were utilized as the heat transfer fluids in the STHE. With the original baffle design, the results showed that at mass flow rate of 2 kg/s, Solar Salt, Hitec, and NaKCaNO3 exhibited the highest pressure drops of 10.051, 10.128, and 9.651 kPa, respectively. The pressure drops were reduced to 5.820, 5.864, and 5.557 kPa, respectively, with the new 6 mm holed baffles. The modified baffles significantly reduced the pressure drop by up to 42 % compared to the original design, with only a minor reduction in the heat transfer coefficient, approximately 17 %. Further analysis revealed a remarkable efficiency improvement of up to 60 % in the modified STHE. The introduction of holes to the baffles substantially lowered the pumping power required for STHE operation. The efficiency improvement achieved through pressure drop reduction significantly outweighs the minor decrease in the heat transfer coefficient. Based on these results, it can be concluded that the heat transfer performance of molten salts in the new modified baffle design of STHE can further improve the efficiency of concentrated solar power (CSP) systems by optimizing thermal management and minimizing energy losses.

1. Introduction

Solar energy stands out as a pivotal renewable energy source, highly favoured for its abundant availability and the vast potential for energy capture. According to National Aeronautics and Space Administration (NASA), the earth is bathed in a staggering 44 quadrillion watts of power in a year, which is akin to the combined output of 44 million power plants, each churning out 1 billion watts per year (Aeronautics and Sun,

E-mail address: gs59765@student.upm.edu.my (M.A. Khaliquzzama).

f Institute of Sustainable Energy, Universiti Tenaga Nasional, 43000 Kajang, Selangor, Malaysia

^{*} Corresponding author.

2005). Research suggests that harnessing the abundant sunshine in some region with intense direct solar radiation could yield approximately 120 GWh of electricity annually from just an area of 1 $\rm km^2$. This level of energy production from solar power is on par with the yearly output of a conventional 50 MW coal or natural gas power plant (Mike, 2009). The immense influx of solar energy presents an unparalleled opportunity for harnessing a clean, inexhaustible power supply that could revolutionize our energy consumption patterns and pave the way towards a sustainable future.

Presently, there are two popular methods employed to harness solar energy for electricity generation which are solar photovoltaic (PV) and concentrated solar power (CSP) (Dudda and Shin, 2013). Solar PV directly transforms sunlight into electricity. Renowned for its adaptability, PV technology is the most widely adopted form of solar energy electricity harvesting globally (Renewables, 2020). It can be seamlessly integrated into compact spaces or scaled up for expansive solar farms. Around 25 percent of all electricity needs are expected to be met by solar PV technology by 2050, with the biggest installed capacity of 8519 GW (Pourasl et al., 2023). The second method, CSP, leverages the sun's thermal energy to generate electricity. In CSP systems, mirrors reflect and concentrate sunlight onto a receiver, where fluids are heated to elevated temperatures. These superheated fluids then drive an electric generator to produce electricity, completing the energy conversion process. In contrast to solar PV systems, CSP systems boast the significant advantage of integration with thermal energy storage. This synergy effectively addresses the issue of solar power's intermittent nature, which arises from fluctuations in weather and daylight hours (Pelay et al., 2017). Moreover, it mitigates the disparity between the timing of energy supply and demand. Consequently, this pairing enhances the overall performance and reliability of electricity generation, ensuring a steadier and more predictable power output (Hu et al., 2019; Han et al., 2020).

The most well-known and widely used heat exchanger in CSP is the shell and tube heat exchanger (STHE), which comes in a variety of forms. This heat exchanger is an indirect contact type, offering several benefits such as a wide surface area, high pressure capabilities, and easy maintenance (Paikar et al., 2024). Efficiency of the heat exchanger relies on numerous factors such as the temperature difference between the cold and hot fluids, heat exchange surface area and flow rates of the fluids. The efficiency can be improved through modification of the fluids, flow conditions and the design of the heat exchanger. Geometric modifications to the length, number of tubes and diameter can be done on the heat exchanger in order to improve its performance (Jadhav and Koli, 2014). In the realm of heat exchanger efficiency, pressure drop emerges as a critical factor. Elevated pressure drop demands more pumping power, which escalates operational costs. Thus, achieving the sweet spot between heat transfer efficiency and manageable pressure drop is essential for optimal performance. Ambekar et al. (Ambekar et al., 2016) investigated performance of different baffle types in STHE and found that heat transfer coefficient (HTC) and pressure drop (PD) was highest with single segmental baffle. Ben Slimene et al. (Ben et al., 2022) studied the performance of rectangular shaped STHE and reported that it performed better when equipped with baffles. You et al. (You et al., 2012) examined STHE equipped with flower type baffle and reported that the heat transfer performance is better than STHE with segmental baffle. Wang et al. (Wang et al., 2018) used segmental, staggered and continuous helical baffles and found that segmental baffles showed superior thermal performance compared to other baffles. Duan et al. (Duan et al., 2016) studied STHE with different angles of helical baffle. To evaluate the STHE performance, ratio of heat transfer performance to pressure drop was compared. They found that the angle of 40 degrees exhibited the best heat transfer performance. Dong et al. (Dong et al., 2017) investigated trisection helical baffles SHTX with few inclination angles and found that 20 degrees has optimum performance while 10 degrees give maximum heat transfer at the cost of high pressure drop. Shinde and Pancha (Shinde and Pancha, 2012) studied helical

baffle STHE with few inclination angles. They found that helical baffle STHE with 15 and 25 degrees gave higher heat transfer performance and lower pressure drop compared to segmental baffles. Azar et al. (Tasouji Azar et al., 2014) studied the performance of helical baffles STHE. They found that helical baffles significantly reduce the pressure drop, but the heat transfer performance is superior with segmental baffles.

The efficiency of CSP plants is highly dependent on the performance of their heat transfer fluids (HTFs) and thermal energy storage (TES) systems. These components are crucial for both generating electricity and storing energy effectively. Molten salts are extensively utilized as the HTF and TES material in CSP systems globally (Awad et al., 2018). It boasts a low vapor pressure, which minimizes the likelihood of pressurerelated incidents, enhancing the safety of CSP operations. Molten salts are able to facilitate CSP systems' operation at a broader range of higher temperatures, allowing a more efficient system performance (Kuchibhotla et al., 2020; Singh et al., 2018). Additionally, molten salt is readily available and cost-effective. Molten salts, while advantageous for high-temperature applications, tend to generate higher pressure drops compared to conventional fluids like oil and water due to their high density and viscosity. These properties increase flow resistance, necessitating greater pumping power to maintain desired flow rates. Another notable challenge is the lack of extensive data on the heat transfer performance of molten salts at elevated temperatures, largely due to the complexities and technical difficulties associated with experimental investigations under the high operating conditions required for CSP systems. The lack of data may cause delayed innovations, challenge in optimizing CSP system, and inefficient CSP operation as the system may operate below their potential efficiency. In response to these gaps, this study aims to reduce the pressure drop in the system, evaluate and report the heat transfer performance of molten salts at elevated temperatures. For this purpose, a new design of segmental baffles with small round holes was proposed for a shell and tube heat exchanger model which was built upon prior research by Ozden and Tari (Ozden and Tari, 2010). and P. Cruz et al. (Cruz et al., 2022). The model focuses on the shell side analysis by using computational fluid dynamics (CFD). To establish a baseline, the model was initially validated using water as the HTF. This step ensures consistency with existing studies and provides a reference for subsequent analyses. Then, the heat transfer performance of molten salt nitrates, specifically Solar salt and Hitec were investigated along with a novel ternary nitrate NaKCaNO₃ reported by Li. et al. (Li et al., 2022). Additionally, the resulting pressure drop in the heat exchanger with the new small round holed segmental baffles was rigorously tested against the original segmental baffles. By strategically altering the segmental baffle design, the aim was to reduce pressure drop and increase the system efficiency. The resulting performance differences were evaluated, shedding light on the trade-offs between heat transfer performance and pressure drop.

2. Methodology

Molten salts can function as heat transfer fluids in Concentrated Solar Power (CSP) systems only when it is in the liquid state. Given their high melting points, molten salts operate as heat transfer fluids exclusively at elevated temperatures. Studying material properties under such extreme conditions is both challenging and hazardous. To address this issue, this study employs Computational Fluid Dynamics (CFD) to analyse the heat transfer properties of molten salts within a shell and tube heat exchanger.

The CFD can be categorized into three general simulation stages: preprocessing, processing, and post-processing. CFD is an iterative and complex process where the solution accuracy is highly dependent on the pre-processing and the processing stage. Each unique setup yields a distinct outcome and through post-processing, visualizing these outcomes and extracting quantitative data can provide guidance to increase solution accuracy. During pre-processing stage, the problem is defined clearly. The shell and tube heat exchanger geometry are modelled with

 Table 1

 Shell and tube heat exchanger geometry dimensions.

0 0 1		
Parameters	Dimensions	
Shell outer diameter (mm)	90	
Nozzle diameter (mm)	36	
Heat Exchanger length (mm)	600	
Tube outlet diameter (mm)	20	
Number of tubes	7	
Tube bundle geometry	Triangular	
Pitch (mm)	30	
Number of baffles	6	
Thickness of baffles (mm)	4	
Central baffle spacing (mm)	86	
Baffle cut (%)	36	

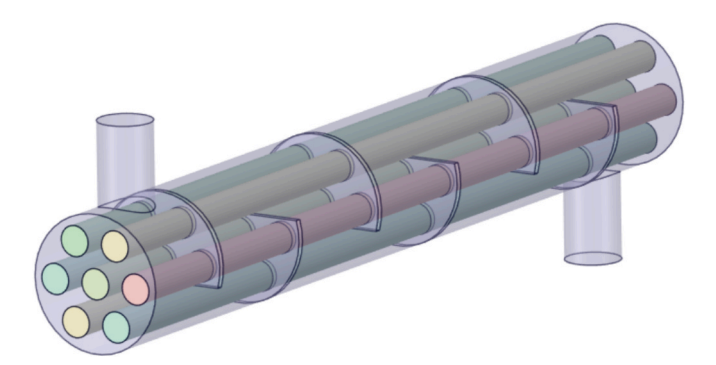


Fig. 1. Geometry of the shell and tube heat exchanger.

the correct dimensions and high-quality corresponding mesh is generated. Subsequently, in the processing stage, the model's governing equations, interfaces, materials, boundary conditions, and cell zone conditions are specified. The calculated results are then gathered and viewed in the post-processing stage, offering improved visualizations. To increase accuracy and produce better results, this three-step process is repeated with different boundary conditions and parameters. The program utilized for the three-step procedure in this investigation is ANSYS. The problem set up parameters and associated dimensions are all adapted from earlier research done by Ozden and Tari (Ozden and Tari, 2010) and Cruz et al. (Cruz et al., 2022) as a basis for validation and data comparison. Solver used for this study is ANSYS-Fluent which solves the governing equations of heat transfer and fluid flow through the finite volume method.

2.1. Pre-processing

2.1.1. Geometry creation

The geometry of the shell and tube heat exchanger is based on the work done by Ozden and Tari (Ozden and Tari, 2010) which was designed following the Tubular Exchanger Manufacturers Association (TEMA) standards which have been validated experimentally. The geometry was created using ANSYS Space Claim. The simplified geometry was build based on the targeted analysis which is for the shell side analysis. Therefore, in this simplified model, the tubes are represented as solid cylinders with a constant temperature. Baffles are modelled by cutting off the baffle dimensions from the shell body. The key design parameters are listed in Table 1 while the simplified model of the shell and tube heat exchanger is shown in Fig. 1. The baffle cut of 36 % was chosen to position the cut slightly below or above the central rows of tubes. The baffle spacing of 86 mm was chosen to align with previously reported studies, enabling straightforward comparison.

2.1.2. Meshing

The meshing was done using ANSYS meshing client, utilizing a mix of tetrahedral and hexahedral cells. The preference for hexahedral

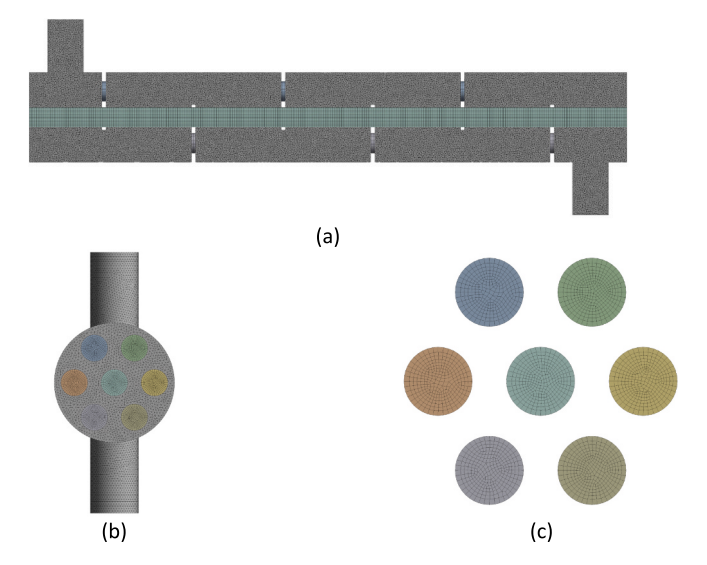


Fig. 2. Cross sectional area meshing for Shell and Tube Heat Exchanger Mesh (a) Side view, (b) Front view, (c) Tubes view.

meshing of the tubes was due to its superior mesh quality over tetrahedral. Mesh density was increased near the wall region through face sizing to better capture the steep gradients of velocity and temperature, while body sizing governs the overall mesh element size. Inflation was applied for both the shell and tube to reduce numerical errors and improve the reliability of the results. Multizone meshing was applied exclusively to the tubes to create a structured hexahedral mesh. The tubes received a finer mesh compared to the shell, balancing the reduction of element count with the maintenance of accuracy. Multiple meshing iterations were conducted to evaluate the trade-off between element number, mesh quality, and the results produced. The outcomes were then compared with the work done by Ozden and Tari (Ozden and Tari, 2010) for model validation.

Fig. 2 showcases the mesh for one set of meshing parameters for the heat exchanger. Fig. 2(a) depicts the meshing of the STHE cross-section from the side view, Fig. 2(b) shows the meshing from the front view, and Fig. 2(c) focuses on the meshing of the individual tubes within the STHE. Different meshing parameters were altered during the mesh creation process to conduct grid independence test. The mesh node and element numbers are listed together with the resulting shell outlet temperature (T_0) in Table 3. The data in the table were then used to determine the grid independence for optimal simulation configuration.

2.2. Processing

2.2.1. Governing equations

A few CFD studies of shell and tube heat exchangers served as the basis for the equation, parameters, and models that are addressed here. The ANSYS Fluent solver, which was used to execute the simulations, has built-in functions for all the equations described in this section. The study was conducted in the steady state to investigate the heat exchanger performance once thermal equilibrium reached, causing the time dependent parameters to be dropped out of all the equations. The resulting equations are described:

2.2.2. Mass conservation equation

In the steady state, the flow rate of fluid entering the heat exchanger is similar to the flow rate of fluid exiting the heat exchanger. Therefore, mass conservation can be applied. The simplified mass conservation equation is:

$$\nabla \cdot (\rho \overrightarrow{V}) = 0 \tag{1}$$

where ∇ is the divergence, ρ is the fluid density and \overrightarrow{V} is the fluid velocity vector.

2.2.3. Momentum conservation equation

Momentum conservation equation is a fundamental principle used in describing the fluid motion. It is part of the Navier-Stokes equation which were derived from Newton's second law of motion. The momentum conservation equations are:

$$x - momentum : \nabla \cdot (\rho u \overrightarrow{V}) = -\frac{\partial \rho}{\partial x} + \frac{\partial \tau_{xx}}{\partial x} + \frac{\partial \tau_{yx}}{\partial y} + \frac{\partial \tau_{zx}}{\partial z}$$
 (2)

$$y - momentum : \nabla \cdot (\rho v \overrightarrow{V}) = -\frac{\partial \rho}{\partial y} + \frac{\partial \tau_{xy}}{\partial x} + \frac{\partial \tau_{yy}}{\partial y} + \frac{\partial \tau_{zy}}{\partial z} + \rho g \tag{3}$$

$$z - momentum : \nabla \cdot (\rho w \overrightarrow{V}) = -\frac{\partial \rho}{\partial z} + \frac{\partial \tau_{xz}}{\partial x} + \frac{\partial \tau_{yz}}{\partial y} + \frac{\partial \tau_{zz}}{\partial z}$$
(4)

where ∇ is the divergence, ρ is the fluid density, \overrightarrow{V} is the fluid velocity vector, τ is the viscous stress in the fluid.

2.2.4. Energy conservation equation

The energy conservation equation expresses that the total energy entering the heat exchanger is the same as the total energy leaving it. The energy conservation equation is:

$$\nabla \cdot (\rho e \overrightarrow{V}) = -p \nabla \cdot \overrightarrow{V} + \nabla \cdot (k \nabla T) + q + \Phi$$
 (5)

where ∇ is the divergence, ρ is the fluid density, \overrightarrow{V} is the fluid velocity vector, ∇T is the temperature difference between hot and cold fluids, q is the heat flux and Φ is the dissipation function.

The dissipation function, Φ in equation (5) can be calculated from equation (6) below (Ozden and Tari, 2010):

$$\Phi = \mu \begin{bmatrix} 2\left[\left(\frac{\partial u}{\partial x}\right)^{2} + \left(\frac{\partial v}{\partial y}\right)^{2} + \left(\frac{\partial w}{\partial z}\right)^{2}\right] + \\ \left(\frac{\partial u}{\partial y} + \frac{\partial v}{\partial x}\right)^{2} + \left(\frac{\partial u}{\partial z} + \frac{\partial w}{\partial x}\right)^{2} + \left(\frac{\partial v}{\partial z} + \frac{\partial w}{\partial y}\right)^{2} \end{bmatrix} + \lambda \left(\nabla \cdot \overrightarrow{V}\right)^{2}$$
(6)

2.2.5. Turbulence model

In this study, the flow was turbulent even at the lowest flow rate of 0.5 kg/s, necessitating the consideration of turbulence effects. The selection of a turbulence model is pivotal in computational fluid dynamics (CFD) research, yet there lacks a universal standard for model choice. Suitability varies per study, often demanding an iterative approach of trial and error. Previous research has indicated that the realizable k-ɛ model, coupled with a first-order discretization scheme, yields high accuracy. Consequently, this model had been selected to advance the investigation in this study.

The transport equation of the realizable k- ϵ model that approximates the dissipation rate (ϵ) is given by Equation (7).

$$\frac{\delta}{\delta x_{j}} (\rho \varepsilon u_{j}) = \frac{\delta}{\delta j} \left\{ \left(\mu + \frac{\mu_{t}}{\sigma_{\varepsilon}} \right) \frac{\delta \varepsilon}{\delta x_{j}} \right\} + \rho C_{1} S \varepsilon + C_{1\varepsilon} \left(\frac{\varepsilon}{k} \right) C_{3\varepsilon} G_{b} - C_{2} \rho \left[\frac{\varepsilon^{2}}{k + \sqrt{\varepsilon v}} \right] + S_{\varepsilon}$$
(7)

The model constants values are:

$$C_{1\varepsilon} = 1.44C_2 = 1.90\sigma_{\varepsilon} = 1.20\sigma_k = 1.0.$$

2.2.6. Boundary conditions

This study employs two distinct sets of boundary conditions. The first set of boundary conditions were adopted from Ozden and Tari (Ozden and Tari, 2010) and utilized to model the heat exchanger using water as

Table 2
Boundary conditions for water and molten salts.

Operating conditions	Heat transfer fluid	Heat transfer fluid		
	Water	Molten salt		
Shell inlet temperature (K)	300	500		
Wall temperature (K)	450	650		
Mass flow rate (kg/s)	0.5, 1.0, 2.0	0.5, 1.0, 2.0		

Table 3Meshing density and the resulting shell outlet temperature (To).

Number of Elements	Number of Nodes	T _o (K)	T _o Difference (%)
307,625	85,819	332.16	Baseline
533,437	165,824	332.68	0.15
1,192,108	415,660	335.47	0.84
1,591,042	532,355	335.68	0.06
1,985,954	629,473	335.67	0.00
3,134,044	920,558	335.78	0.03

the heat transfer fluid for validation purpose. The second boundary condition set was used to replace molten salt as the heat transfer fluid, where higher operating temperature is required due to the high melting point of the salt. The specific boundary conditions for both cases are delineated in Table 2.

2.3. Post-processing

In this study, post-processing encompasses both result visualization and quantitative analysis. ANSYS's integrated functions are employed to generate temperature, velocity, and pressure contours, which illustrate the fluid dynamics within the heat exchanger, highlighting flow patterns and areas of interest. Quantitative analysis involves calculating the heat transfer area, temperature gradient, heat flux, and the heat transfer coefficient. The combination of visual and numerical data provides a comprehensive insight into the fluid flow and heat transfer performance.

The overall heat transfer coefficient, U, can be calculated from equation (8) and the heat transfer rate, \dot{Q} can be calculated from equation (9).

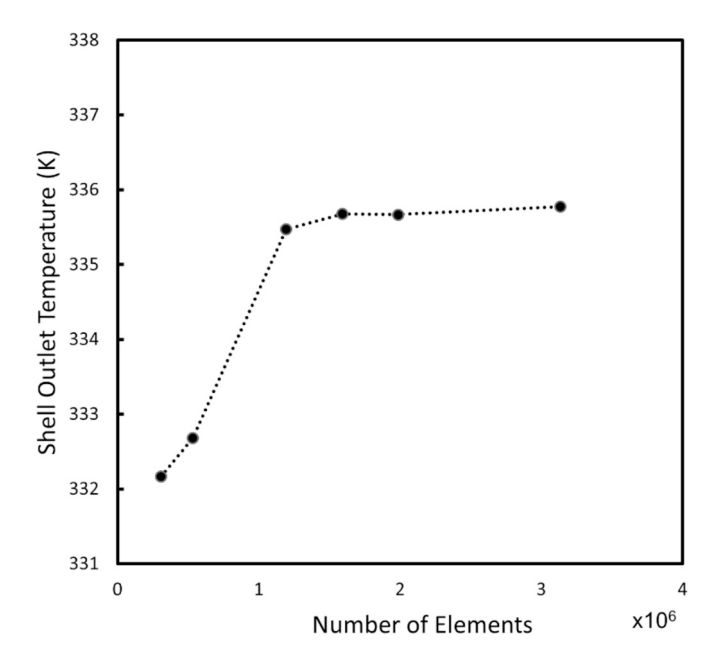


Fig. 3. Grid independence study based on variation of shell outlet temperature with number of elements.

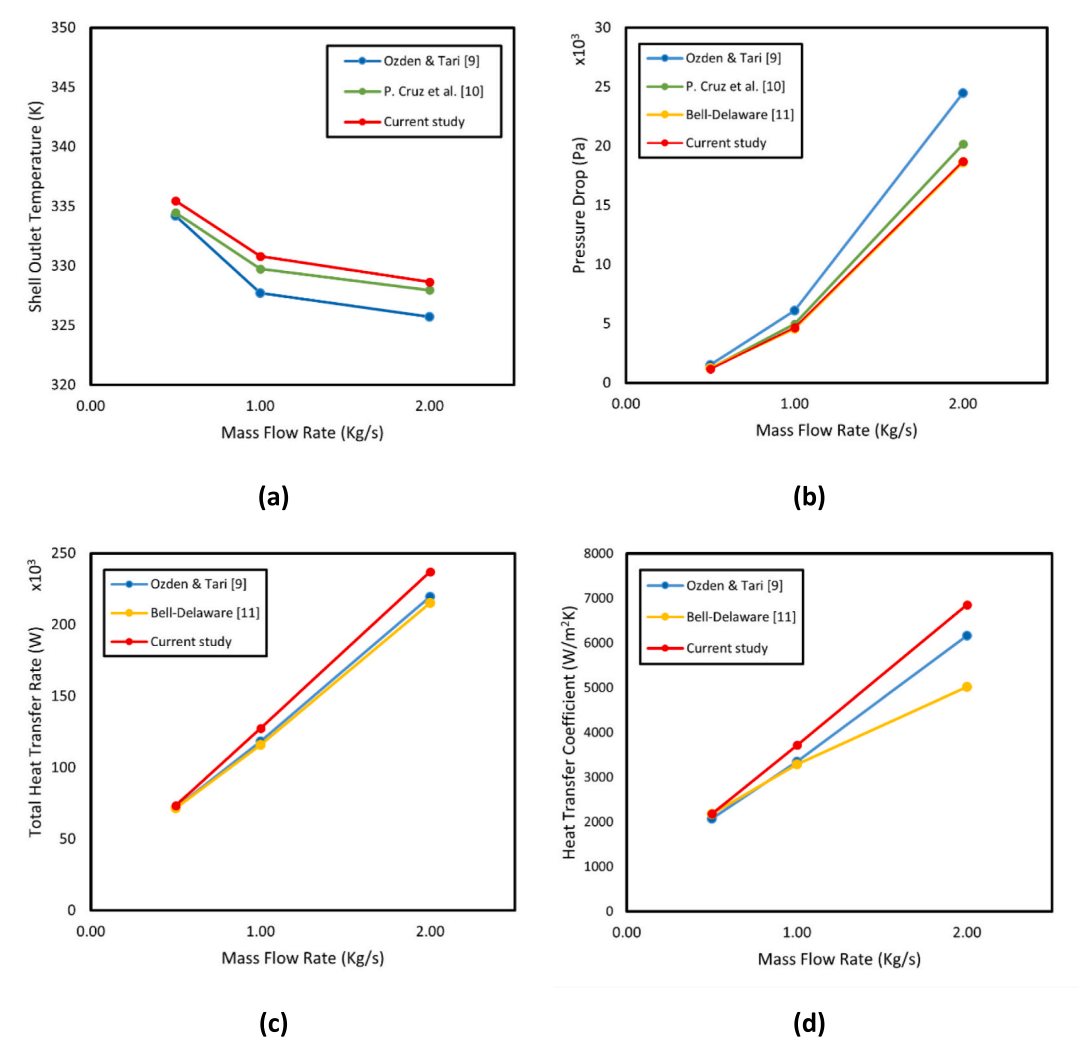


Fig. 4. Model validation of current study using mass flow rates effect on (a) shell outlet temperature, (b) pressure drop, (c) total heat transfer rate, (d) heat transfer coefficient.

$$U = \frac{\dot{Q}}{A \times LMTD} \tag{8}$$

$$\dot{Q} = \dot{m}C_p(T_o - T_i) \tag{9}$$

where A is the total surface area where heat transfer takes place, LMTD is the log mean temperature difference for the counter flow heat exchanger, \dot{m} is the mass flow rate of fluid, C_p is the fluid specific heat capacity, T_o is the shell outlet temperature and T_i is the shell inlet temperature.

2.4. Grid independence study

To achieve the most accurate result while optimizing simulation time, a grid independence study was meticulously conducted. This study evaluated six distinct mesh configurations, each varying in the number of mesh elements. The shell outlet temperature was selected as the primary metric for this assessment, as it serves as the most critical indicator of the heat exchanger's performance. Each of the six mesh configurations, detailed in Table 3 was systematically examined and graphically represented in Fig. 3 to illustrate the effect of mesh refinement on temperature variation. This approach provided valuable insights into the trade-offs between accuracy and computational cost, ensuring a robust and reliable simulation setup.

Beyond an element count of 1,192,108, further increases in mesh

resolution had a negligible impact on temperature variation, with the associated error remaining below 0.1 %. This indicates that grid independence was effectively achieved at this threshold, ensuring that additional refinement would not yield significant improvements in accuracy. Consequently, the 1,192,108-element configuration was selected as the optimal mesh for this study, as it strikes a balance between computational efficiency and precision in thermal analysis.

2.5. Validation of the CFD model

The validation of the CFD model is a critical step to evaluate the accuracy of the created model. An effective model should align closely with either the experimental data, theoretical values, or a previously verified CFD models. In this study, the model validation was done through comparison with previously verified experimental data and CFD modelling by Ozden and Tari (Ozden and Tari, 2010), P. Cruz et al. (Cruz et al., 2022) and numerical data using Bell-Delaware (Bell et al., 1981) method. This comparative analysis serves to reinforce the credibility of the model and ensure its reliability in simulating real-world scenarios.

The validation study was carried out for 3 different water mass flow rates, which were 0.5, 1.0 and 2.0 kg/s. Fig. 4 compares the result of current study to the values reported by Ozden & Tari (Ozden and Tari, 2010), P. Cruz et al. (Cruz et al., 2022) and Bell-Delaware (Bell et al., 1981) calculation. In general, the value reported in this study follows the trend reported by the other studies. As mass flow rates increase, a

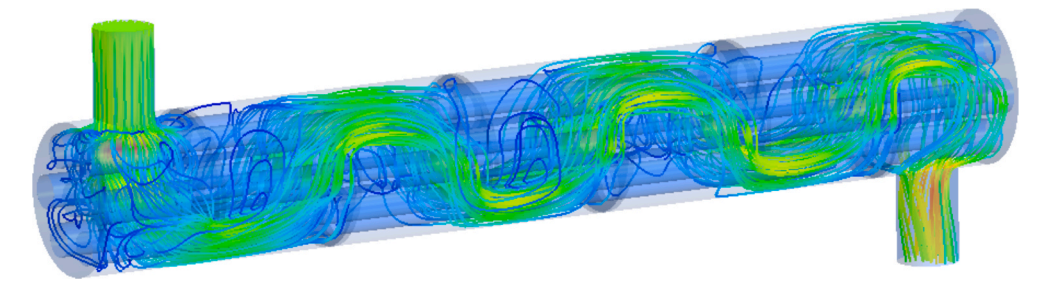


Fig. 5. Velocity streamline flow inside heat exchanger using water on the existing baffle design.

decrease in shell outlet temperature alongside an increase in pressure drop, total heat transfer rate, and heat transfer coefficient was observed. At 0.5 kg/s, the measured shell outlet temperature closely aligns with values reported by Ozden & Tari (Ozden and Tari, 2010) and P. Cruz et al. (Cruz et al., 2022). At 1.0 kg/s and 2.0 kg/s, the shell outlet temperature measured closely resembles those of P. Cruz et al. (Cruz et al., 2022) with a slight deviation from Ozden & Tari (Ozden and Tari, 2010). The deviation of shell outlet temperatures measured in this study to that of Ozden & Tari (Ozden and Tari, 2010) is around 4–11 %, while the difference compared to P. Cruz et al. (Cruz et al., 2022) is less than 4 % for all the mass flow rates.

The pressure drop measured was very close to the value obtained using Bell-Delaware method (Bell et al., 1981), and differs slightly to P. Cruz et al. (Cruz et al., 2022). A higher pressure drop difference were observed when compared to Ozden & Tari (Ozden and Tari, 2010), around 23 % for all mass flow rates. The total heat transfer and heat transfer coefficient were not reported by P. Cruz et al. (Cruz et al., 2022). The total heat transfer rate and heat transfer coefficient obtained were slightly higher but follows the same trendline with Ozden & Tari (Ozden and Tari, 2010) and Bell-Delaware method (Bell et al., 1981) except for 2.0 kg/s where Bell-Delaware method (Bell et al., 1981) deviates slightly from the trend. The total heat transfer rate differences were less than 10% while heat transfer coefficient differences were less than 13 % compared to both Ozden & Tari (Ozden and Tari, 2010) and Bell-Delaware method (Bell et al., 1981) except at 2.0 kg/s where Bell-Delaware method (Bell et al., 1981) differs by around 36 % for the heat transfer coefficient.

Overall, the values reported in this study closely align with other studies, with minor differences attributable to variations in geometry creation and meshing methods. The absence of sudden spikes in results diverging from the trend underscores the robustness of the model developed in this study, making it a suitable foundation for further analysis.

3. Results and discussion

3.1. Velocity streamline flow inside heat exchanger

Fig. 5 shows the velocity streamline flow of fluid inside the heat exchanger with the existing design. The fluid flows from the shell inlet, through the heat exchanger baffles and tubes outer, towards the shell outlet. The presence of baffles in the heat exchanger causes a zig-zag flow pattern as seen in the figure. These baffles promote turbulence inside the shell and tube heat exchanger. The baffles allow for more mixing to occur, creating vortices and swirls which in return enhance the heat transfer. In the report by B. Du et al. (Du et al., 2017), heat transfer performance of shell and tube heat exchangers with baffles were found to be superior than the heat exchanger without baffles, especially in low Re region. Increased heat transfer performance in heat exchangers with baffles has also been reported by several other researchers such as Ben Slimane et al. (Ben et al., 2022) in their study on rectangular STHE, J. Ji et al. (Ji et al., 2023) with elastic bundle tube heat exchanger and Aniket et al. (Ambekar et al., 2016) with the conventional STHE.

Baffles are crucial in controlling fluid behaviour within heat exchangers. Without baffles, fluid encounters less resistance, allowing it to flow more easily from the shell inlet to the shell outlet. This situation results in a lower pressure drop within the system but compromises heat transfer performance. Baffle design significantly influences fluid movement inside the STHE, impacting both heat transfer and pressure drop. With the appropriate design tailored to the application, baffles can help strike a balance between enhancing heat transfer and maintaining an acceptable pressure drop within the system.

3.2. Design modification of the heat exchanger baffle

In this study, a new baffle design was proposed by adding 12 small holes to the existing design, as shown in Fig. 6. The primary goal of this modification was to increase the flow area for the fluid, thereby reducing the pressure drop within the system. It is important to note that pressure drop significantly affects the operational cost of a heat

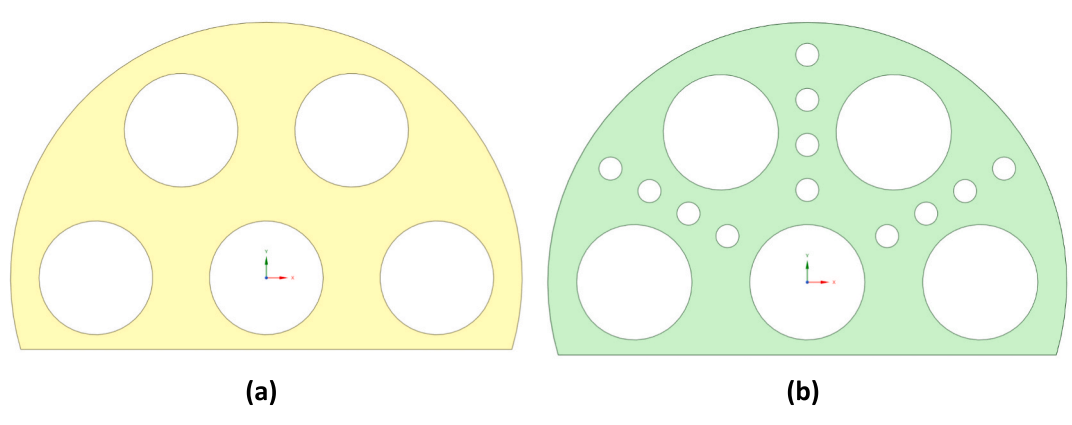


Fig. 6. Baffle design of (a) original baffle, (b) modified baffle.

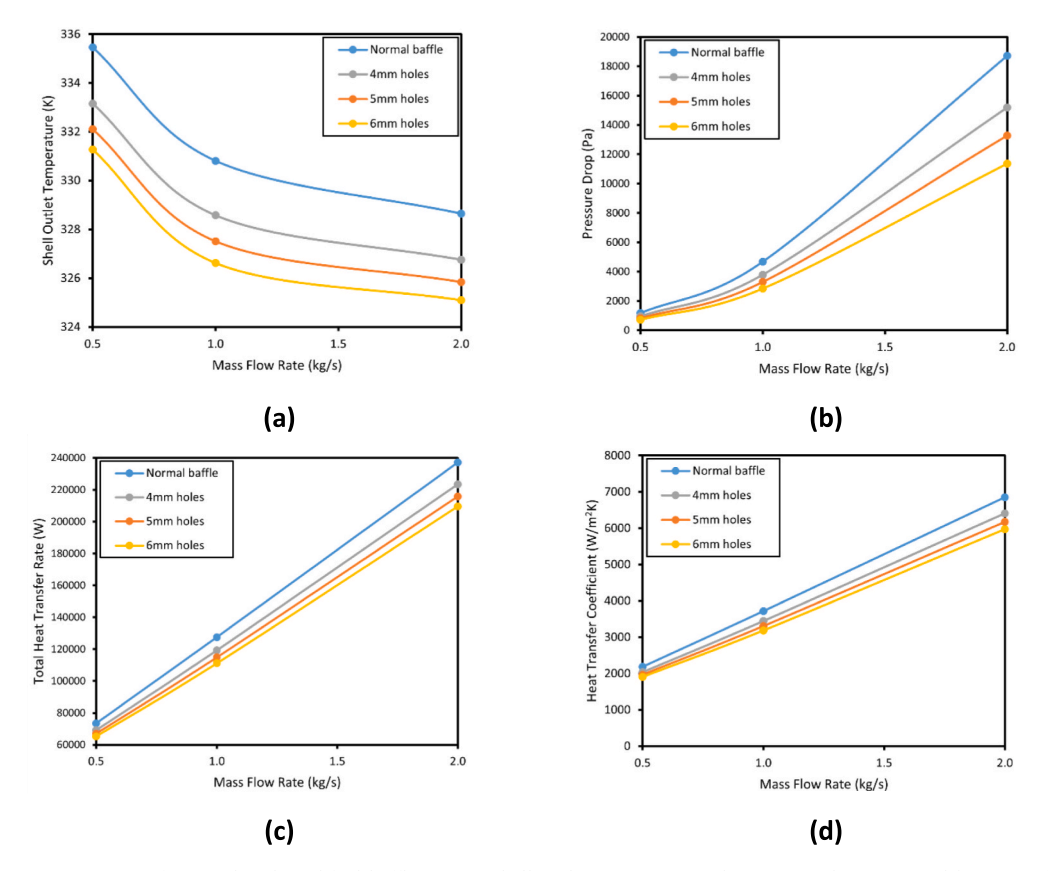


Fig. 7. Performance comparison of original and modified baffles on (a) shell outlet temperature, (b) pressure drop, (c) total heat transfer rate, (d) heat transfer coefficient.

Table 4
Heat transfer performance of water inside shell and tube heat exchanger with original and modified baffles

original and modified buries.							
Baffle Design	Mass Flow Rate (kg/s)	Shell Outlet Temperature (K)	Pressure Drop (Pa)	Total Heat Transfer Rate (W)	Heat Transfer Coefficient (W/m ² K)		
Original	0.5	335.47	1165	73,407	2182		
Baffles	1.0	330.81	4673	127,506	3719		
	2.0	328.65	18,714	237,122	6856		
4 mm	0.5	333.16	946	69,245	2037		
holes	1.0	328.58	3784	119,380	3448		
	2.0	326.76	15,181	223,579	6412		
5 mm	0.5	332.11	825	67,065	1965		
holes	1.0	327.51	3297	114,940	3306		
	2.0	325.84	13,266	215,921	6170		
6 mm	0.5	331.28	706	65,319	1907		
holes	1.0	326.62	2839	111,195	3187		
	2.0	325.10	11,362	209,618	5972		

exchanger. However, any reduction in pressure drop may also impact the overall heat transfer performance.

To explore this further, the heat transfer performance was investigated for different baffle hole diameters: 4 mm, 5 mm, and 6 mm. The pressure drop and heat transfer performance of water in the STHE with various baffle hole sizes were investigated and analysed. Fig. 6 visually compares the original and modified baffle designs. Besides the hole's introduction, other specification of the baffles such as thickness, size and baffle cuts are maintained the same.

3.3. Effect of baffle holes to the pressure drop and heat transfer performance

The heat transfer performance of water in the STHE with both the original and modified baffles are visualized in Fig. 7 while the detailed value can be found in Table 4. The data showed a consistent trend when comparing the original and modified baffles. As the mass flow rate increased, the shell outlet temperature decreased. The highest shell outlet temperature was recorded with the original baffle. Conversely, as the hole size of the modified baffles increased, the shell outlet temperature decreased. This trend was reversed for the pressure drop values, where an increase in mass flow rate led to higher pressure drops. This is expected as higher mass flow rate increases the fluid velocity and turbulence, resulting in higher pressure drop in the system. The original unmodified baffles exhibited the highest pressure drop in all condition. For the modified baffles, larger hole sizes resulted in lower pressure drops as more fluid are allowed to pass through the baffles. The total heat transfer rate and heat transfer coefficient increases with increasing mass flow rates. The highest heat transfer values were observed with original baffles, and the value drops with modified baffles. As the hole size of the modified baffles increase, the total heat transfer rate and heat transfer coefficient decreased. This decrement can be attributed to lower resistance in the fluid flow, reducing the turbulence and fluid mixing.

The introduction of holes to the baffles changes the way fluid flow inside the heat exchanger. Fig. 8 compares the velocity profile of fluid flow for the same mass flow rate inside STHE using original and modified baffles. It can be observed that for the original baffles, velocity is intense and concentrated along the zig-zag flow path. For heat exchanger with modified baffles, the velocity is less intense, but the fluid still mainly flows in a zig-zag pattern with some flowing through the holes of the baffles. The fluid passing through the holes in the baffles reduces stagnant, low-velocity areas, as observed in Fig. 8(b). However,

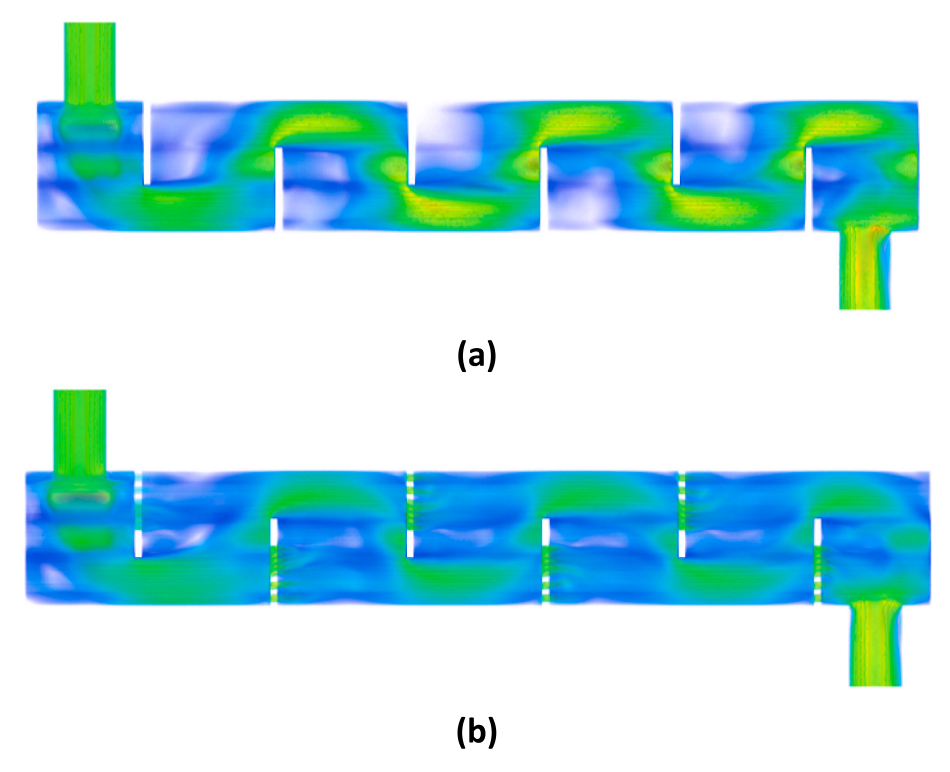


Fig. 8. Velocity profile of fluid inside heat exchanger with (a) original baffle, (b) modified baffle.

Table 5Operating condition for molten salt in STHE.

Operating conditions	Value
Shell Inlet Temperature (K)	500
Wall temperature (K)	650
Mass Flow Rates (kg/s)	0.5, 1.0, 2.0

this also diminishes turbulence in the system, resulting in decreased heat transfer performance.

3.4. Molten salt Incorporation

The study was continued by replacing water with molten salts as the heat transfer fluid in the STHE to simulate the actual fluid used in CSP. For this purpose, three types of molten salt were chosen due to their wide usage, high potential and suitable for application in CSP plants. The boundary conditions for the simulations are listed in Table 5. The shell outlet temperature and pressure drops are directly obtained from the simulation results. Additionally, the total heat transfer rate and heat transfer coefficients were calculated, and these data are presented in Table 6.

3.4.1. Shell outlet temperature & pressure drop

Fig. 9 and Fig. 10 shows that increasing the mass flow rate from 0.5 to 2.0 kg/s for molten salts also resulted in a decrease of shell outlet temperature and an increase of pressure drop as observed with water. Comparing between the molten salts, Hitec consistently showed higher shell outlet temperatures across all mass flow rates followed by NaK-CaNO3 and lastly solar salt. This can be attributed to the molten salt thermal conductivity. Solar salt has the lowest thermal conductivity amongst the molten salts while NaKCaNO3 has the highest thermal conductivity, in agreement with the shell outlet temperature trend. The pressure drop escalates with an increase in mass flow rates, a trend consistent across all molten salts analysed. Amongst the salts, NaK-CaNO3 exhibited the most favourable behaviour, with the lowest

pressure drop at varying mass flow rates. Solar salt followed closely, demonstrating only a marginally higher pressure drop. Hitec salt, however, showed the most significant pressure drop. These findings can be primarily linked to the molten salt's viscosity. Hitec possesses the highest viscosity, followed by solar salt and then NaKCaNO₃, aligning with the observed pressure drop sequence.

Examining the differences between the original and modified baffles, the original baffle (without holes) exhibits higher shell outlet temperatures and greater pressure drops at all mass flow rates of the molten salts. Although the difference in shell outlet temperature between the original and modified baffles are minimal, the difference in their pressure drop is significant. An unusual phenomenon was observed at mass flow rate of 0.5 kg/s. The modified baffle exhibited an increase in shell outlet temperature as the hole size increased from 4 mm to 6 mm. This trend is unusual and contrasts with observations at mass flow rates of 1.0 and 2.0 kg/s, where larger hole sizes resulted in lower shell outlet temperatures. The observation at 0.5 kg/s might be attributed to fluid movement behaviour at low speeds. As depicted in Fig. 8(b), the fluid predominantly moves in a zig-zag pattern even in the presence of holes. At the mass flow rate of 0.5 kg/s, the pressure of fluid passing through the baffle holes decreases as the hole size increases. These low-pressure fluids may have an insignificant effect on turbulence in the STHE where turbulence might be dominated by the zigzag flowing fluid. Therefore, at a low mass flow rate of 0.5 kg/s, increasing the baffle hole size does not significantly alter the fluid flow, resulting in a slight increase in shell outlet temperature as the hole size increases. However, the trend of the pressure drop values did not change, which decreases as the baffle hole size increases across all mass flow rates.

3.4.2. Total heat transfer rate & heat transfer coefficient

In general, the trend of the total heat transfer rate mirrors that of the heat transfer coefficient. Based on Fig. 11 and Fig. 12, it can be observed that as the mass flow rate increases, the total heat transfer rate and heat transfer coefficient increases. This observation applies to all the molten salts studied. The heat transfer coefficient is intrinsically linked to the fluid's thermal conductivity where a higher thermal conductivity

Table 6
Heat transfer performance of molten salts inside shell and tube heat exchanger with original and modified baffles.

Material	Baffle Type	Mass Flow Rate (kg/s)	Shell Outlet Temperature (K)	Pressure Drop (Pa)	Total Heat Transfer Rate (W)	Heat Transfer Coefficient (W/m²K)
Solar Salt	Original baffle	0.5	538.76	631	27,948	842
		1.0	523.64	2500	34,094	967
		2.0	516.97	10,051	48,958	1354
	4 mm holes	0.5	537.10	509	26,756	800
		1.0	521.85	1956	31,509	887
		2.0	515.31	7832	44,162	1213
	5 mm holes	0.5	537.23	452	26,844	803
		1.0	521.54	1710	31,062	873
		2.0	514.78	6788	42,641	1169
	6 mm holes	0.5	537.33	398	26,917	806
		1.0	521.35	1487	30,792	865
		2.0	514.32	5820	41,301	1130
Hitec	Original baffle	0.5	549.78	645	35,274	1117
	-	1.0	530.05	2531	42,586	1238
		2.0	520.89	10,128	59,220	1661
	4 mm holes	0.5	548.29	521	34,220	1075
		1.0	528.23	1985	40,014	1154
		2.0	518.95	7880	53,721	1495
	5 mm holes	0.5	548.46	463	34,336	1080
		1.0	528.02	1737	39,715	1145
		2.0	518.30	6878	51,857	1440
	6 mm holes	0.5	548.61	409	34,445	1084
		1.0	527.99	1513	39,673	1143
		2.0	517.73	5864	50,238	1392
NaKCaNO ₃	Original baffle	0.5	547.55	603	35,510	1113
		1.0	529.15	2398	43,543	1261
		2.0	521.42	9651	63,990	1799
	4 mm holes	0.5	546.46	481	34,700	1081
		1.0	527.06	1874	40,413	1160
		2.0	519.39	7476	57,918	1615
	5 mm holes	0.5	546.60	423	34,798	1085
		1.0	526.52	1628	39,610	1135
		2.0	518.68	6503	55,809	1552
	6 mm holes	0.5	546.77	371	34,929	1090
		1.0	526.19	1405	39,125	1120
		2.0	517.99	5557	53,749	1491

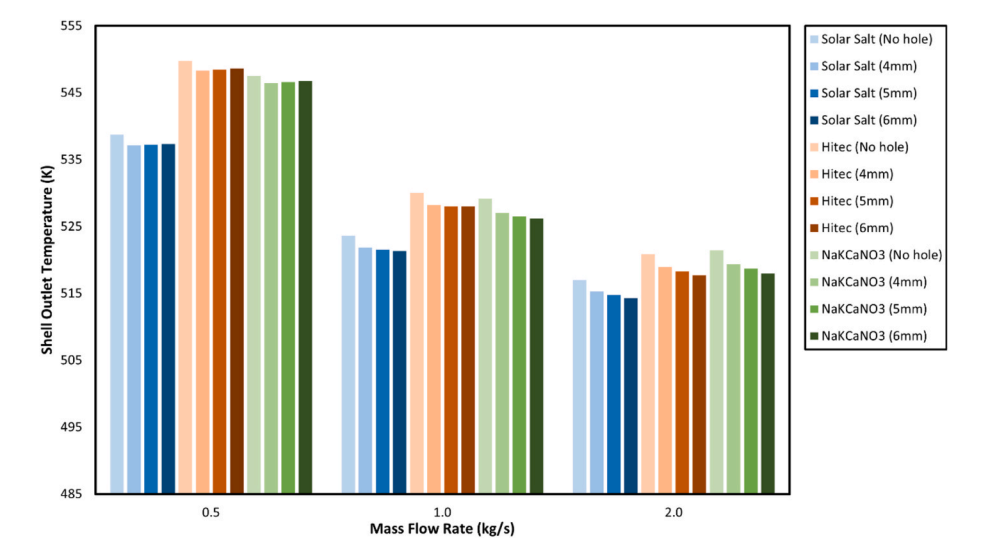


Fig. 9. Shell outlet temperature of molten salts.

typically facilitates greater heat transfer for a given temperature difference. Solar salt, possessing the lowest thermal conductivity among the salts, naturally has the lowest heat transfer coefficient values across the mass flow rates. Hitec and NaKCaNO $_3$ displayed quite close value of heat transfer coefficients at lower flow rates of 0.5 and 1.0 kg/s. However, at higher flow rate of 2.0 kg/s, NaKCaNO $_3$'s heat transfer coefficient significantly exceeded that of Hitec. This divergence can be attributed to each salt's unique thermophysical properties.

At an inlet temperature of 500 K, Hitec thermal conductivity is approximately 13 % higher than that of NaKCaNO $_3$. But, as temperatures rise above 530 K, NaKCaNO $_3$'s thermal conductivity overtakes that of Hitec by a considerable margin. This shift in NaKCaNO $_3$'s thermal conductivity significantly impacts its performance especially at mass flow rate of 0.5 kg/s. At mass flow rates of 1.0 kg/s and 2.0 kg/s, Hitec has higher thermal conductivity value compared to NaKCaNO $_3$ as the maximum temperature of the fluid remains below 530 K. However,

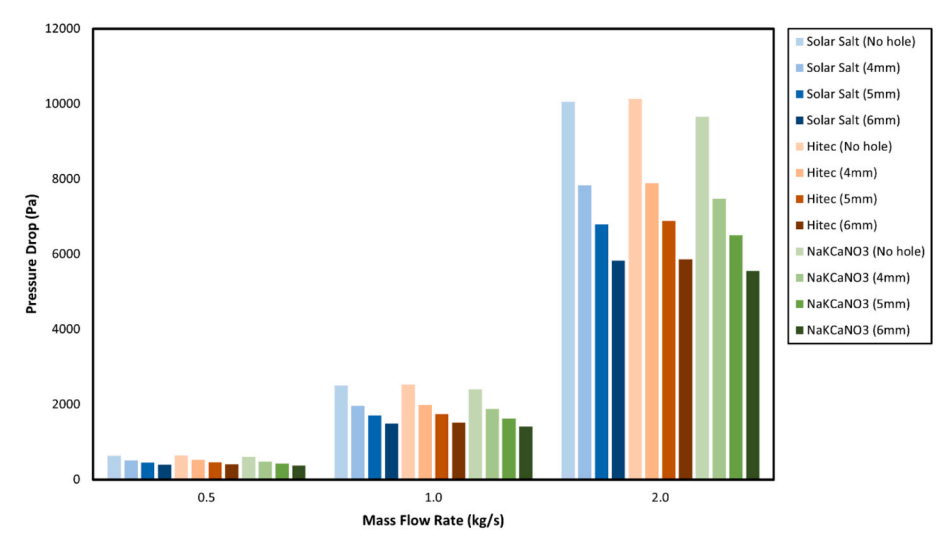


Fig. 10. Pressure drop of molten salts.

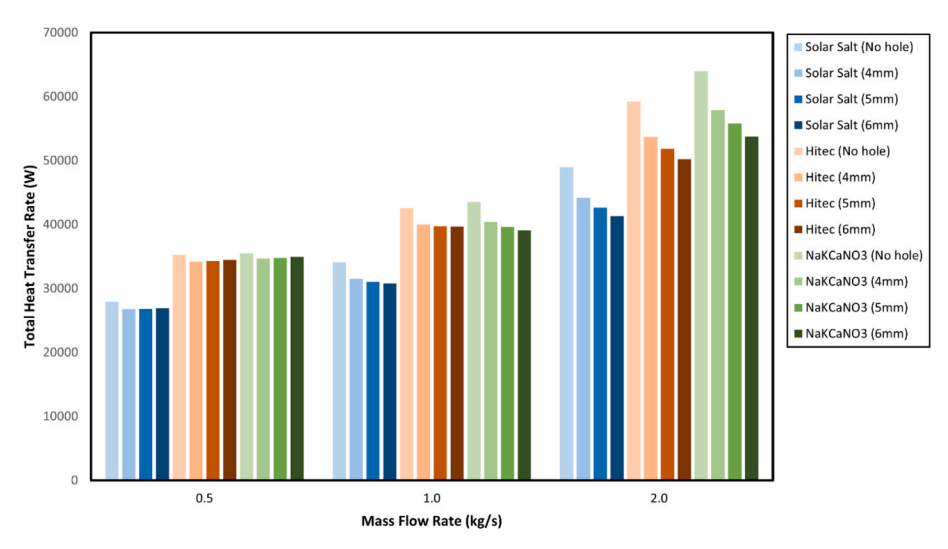


Fig. 11. Molten salts total heat transfer rate.

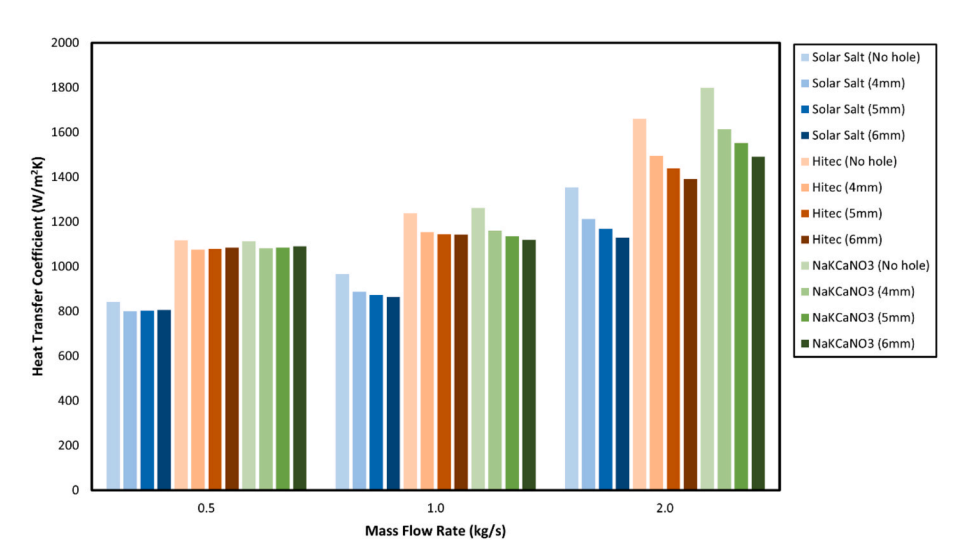


Fig. 12. Molten salt heat transfer coefficient.

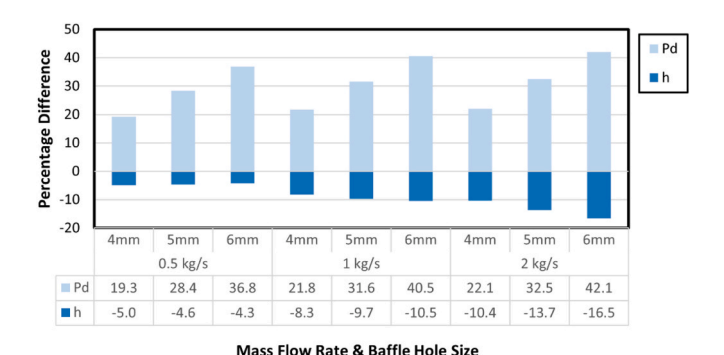
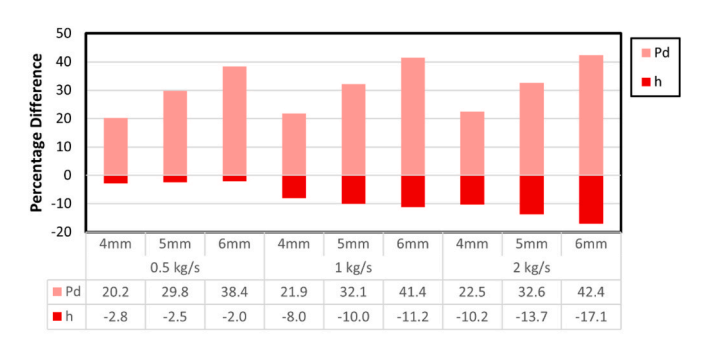


Fig. 13. Impact of pressure drop reduction on heat transfer coefficient of Solar Salt.



Fig. 14. Impact of pressure drop reduction on heat transfer coefficient of Hitec.



Mass Flow Rate & Baffle Hole Size

Fig. 15. Impact of pressure drop reduction on heat transfer coefficient of $NaKCaNO_3$.

 ${
m NaKCaNO_3}$ seems to have better heat transfer performance than Hitec. This discrepancy could be influenced by the specific heat capacity and density of the materials. ${
m NaKCaNO_3}$ has a higher specific heat capacity and density compared to Hitec across all temperatures considered in this study. It becomes evident that the heat transfer coefficient cannot be just related to the thermal conductivity or specific heat capacity value of the material, but it might have multiple dependency and other influencing factors which needs to be investigated further.

Comparing between the original and the modified baffle, the original baffle consistently exhibits the highest values for both the total heat transfer rate and the heat transfer coefficient across all mass flow rates. For the modified baffle, a similar pattern to the shell outlet temperature was observed where at mass flow rate of 0.5 kg/s, the total heat transfer rate and heat transfer coefficient increases with increasing hole diameter. However, the trend reverses at mass flow rates of 1.0 and 2.0 kg/s, where both the total heat transfer rate and the heat transfer coefficient decreases as the hole diameter increases.

3.5. Pressure drop effect on heat transfer performance

This section evaluates the impact of pressure drop reduction on heat transfer coefficient of the modified baffle design. The original baffle without holes serves as the baseline for comparison with the modified baffles, which have hole diameters of 4 mm, 5 mm, and 6 m. The test was conducted for mass flow rates of 0.5 kg/s, 1.0 kg/s, and 2.0 kg/s. Three graphs were generated for the different molten salts: Solar salt, Hitec, and NaKCaNO₃. In these graphs, (Pd) denotes the pressure drop reduction percentage, and (h) represents the heat transfer coefficient percentage of the modified baffles relative to the original baffle design.

Based on Fig. 13–15, the introduction of modified baffles significantly reduced the pressure drop across all types of molten salts, with reductions ranging from 19 % to 42 %. As the mass flow rate increases, the pressure drop reduction also increases. For solar salt with 5 mm baffle holes, the pressure drop reduction increases from 28.4 % to 32.5 % as the mass flow rate rises from 0.5 kg/s to 2.0 kg/s. Larger baffle holes further enhance the pressure drop reduction, with 6 mm holes nearly doubling the reduction achieved by 4 mm holes. The differences in pressure drop between different types of molten salts at the same mass flow rate and baffle holes are minimal, below 2 %. This indicates that the pressure drop in the system relies significantly on the STHE design, with some dependence on the fluid type. Thus, the heat exchanger design is crucial in controlling the pressure drop of STHE.

The reduction in pressure drop is accompanied by a decrease in the heat transfer coefficient. As the mass flow rate increases, the heat transfer coefficient value decreases. At 0.5 kg/s, the heat transfer coefficient increases as the baffle hole size increases from 4 mm to 6 mm, a trend observed for all molten salts studied. This situation is similar as to what discussed above in section 0 where the zigzag flowing fluid effect is significantly higher than the fluid passing through the baffle holes. At 1.0 kg/s and 2.0 kg/s, the heat transfer coefficient reduces with larger baffle hole sizes. When comparing between different molten salt types, the reduction in the heat transfer coefficient is more pronounced at a lower mass flow rate of 0.5 kg/s. As the mass flow rate increases, the differences in heat transfer coefficient reduction between the different salts diminish. For example, at a mass flow rate of 0.5 kg/s with 5 mm baffles, the heat transfer coefficient reduction percentages are 4.6 % for solar salt, 3.3 % for Hitec, and 2.5 % for NaKCaNO3. These values rise to 9.7 %, 7.6 %, and 10 % respectively at 1.0 kg/s, and to 13.7 %, 13.3 %, and 13.7 % respectively at 2.0 kg/s. Therefore, at higher mass flow rates, baffle design significantly impacts the heat transfer coefficient reduction percentage.

3.6. Performance index and overall system efficiency

Heat transfer and pressure drop are interrelated. The performance index (η) of the heat exchanger can be measured using the heat transfer coefficient and its pressure drop values (Taghizadeh-Tabari et al., 2016). With higher values of heat transfer, it is likely that the pressure drop will be higher as well. High pressure drop is not favourable as it means that more pumping power is required to maintain the desired flow which translates into higher operation cost. This section investigates the performance parameter of each case, comparing the ratio of pressure drop to the loss in heat transfer performance. The simple performance index (η) formula is defined below based on previous work by Tabari et al. (Taghizadeh-Tabari et al., 2016). The performance index quantifies the ratio of heat transfer coefficient enhancement relative to the associated pressure drop.

$$\eta = \frac{\frac{h_m}{h_o}}{\frac{Pd_m}{Pd_o}} \tag{10}$$

where h_m is the heat transfer coefficient of modified baffle, h_o is the heat transfer coefficient of original baffle, Pd_m is the pressure drop of modified baffle and Pd_o is the pressure drop of original baffle.

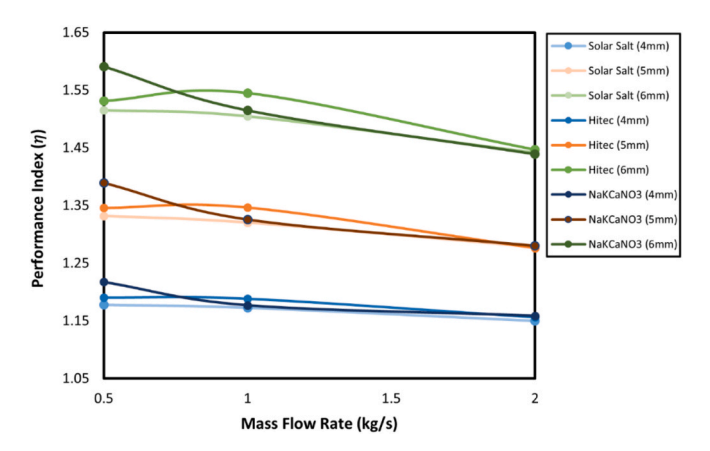


Fig. 16. Performance index (η) comparison of molten salts.

From Fig. 16, it is observed that all the molten salts exhibit a performance index greater than 1 in the modified baffle STHE for all baffle hole sizes. This indicates that, in every case, the pressure drop reduction is significantly greater than the reduction in heat transfer coefficient. The performance index is highest with the 6 mm baffle hole size and lowest with the 4 mm baffle hole size. As the mass flow rate increases, the performance index value decreases for all molten salts, except for Hitec, which has the highest performance index value at 1 kg/s. At a lower mass flow rate of 0.5 kg/s, NaKCaNO₃ has the highest performance index. As the mass flow rate approaches 2 kg/s, all the molten salts exhibit a quite similar performance index value. In summary, the modified baffle significantly reduced the pressure drop compared to the reduction in heat transfer coefficient. However, it is important to strike a

balance between reducing pressure drop and maintaining adequate heat transfer performance, depending on the specific application and requirements. Overemphasis on reducing pressure drop without considering the impact on heat transfer efficiency may render the system inefficient.

3.6.1. Overall system efficiency

The overall efficiency of STHE can be further investigated by performing a hydraulic analysis to better understand its performance. The overall efficiency is assessed by evaluating the energy required for pumping relative to the total heat transfer rate.

$$Efficiency = \frac{Totalheattransferrate(W)}{Pumpingpower(W)}$$
(11)

The pumping power is related to the pressure drop in the STHE. A simple method to calculate the pumping power is as follows:

$$Pumpingpower(W) = Massflowrate \left(\frac{kg}{s}\right) * \frac{Pressuredrop(Pa)}{Fluiddensity\left(\frac{kg}{m^3}\right)}$$
 (12)

The overall system efficiency can be readily calculated using the formula provided, based on the data presented in Table 6. The calculated efficiency is represented as a dimensionless value, while the efficiency improvements are expressed as percentages relative to the original nohole baffle design as detailed in Table 7.

Table 7 highlights that all modified baffles with hole sizes ranging from 4 mm to 6 mm enhanced the overall efficiency of the STHE compared to the original no-hole baffles. Efficiency improvements span from $15\,\%$ to nearly $60\,\%$. The highest gains are observed with the 6 mm baffle holes, achieving more than $45\,\%$ improvement across all molten

Table 7Overall efficiency of the original and modified STHE.

Material	Baffle Type	Mass Flow Rate (kg/s)	Total Heat Transfer Rate, \dot{Q} , (W)	Pumping Power, PP, (W)	Efficiency (\dot{Q}/PP)	Efficiency Improvement (%)
Solar Salt	No Holes	0.5	27,948	0.16	171,328	
		1.0	34,094	1.29	26,351	Baseline
		2.0	48,958	10.40	4707	
4	4 mm	0.5	26,756	0.13	203,227	18.6
		1.0	31,509	1.01	31,131	18.1
		2.0	44,162	8.11	5448	15.8
	5 mm	0.5	26,844	0.12	229,722	34.1
		1.0	31,062	0.89	35,097	33.2
		2.0	42,641	7.02	6070	29.0
	6 mm	0.5	26,917	0.10	261,286	52.5
		1.0	30,792	0.77	40,030	51.9
		2.0	41,301	6.02	6857	45.7
Hitec	No Holes	0.5	35,274	0.17	205,057	
		1.0	42,586	1.35	31,531	Baseline
		2.0	59,220	10.81	5479	
	4 mm	0.5	34,220	0.14	246,022	20.0
		1.0	40,014	1.06	37,775	19.8
		2.0	53,721	8.41	6388	16.6
	5 mm	0.5	34,336	0.12	277,875	35.5
		1.0	39,715	0.93	42,828	35.8
		2.0	51,857	7.34	7065	28.9
6 mm	6 mm	0.5	34,445	0.11	315,947	54.1
		1.0	39,673	0.81	49,148	55.9
		2.0	50,237	6.26	8027	46.5
NaKCaNO3	No Holes	0.5	35510.4	0.15	233,812	
		1.0	43543.4	1.21	36,035	Baseline
		2.0	63989.6	9.73	6580	
	4 mm	0.5	34699.8	0.12	286,270	22.4
		1.0	40413.1	0.94	42,799	18.8
		2.0	57918.2	7.53	7688	16.8
	5 mm	0.5	34798.4	0.11	326,401	39.6
		1.0	39610.3	0.82	48,302	34.0
		2.0	55808.6	6.55	8516	29.4
	6 mm	0.5	34929.4	0.09	373,478	59.7
		1.0	39124.6	0.71	55,267	53.4
		2.0	53748.5	5.60	9598	45.9

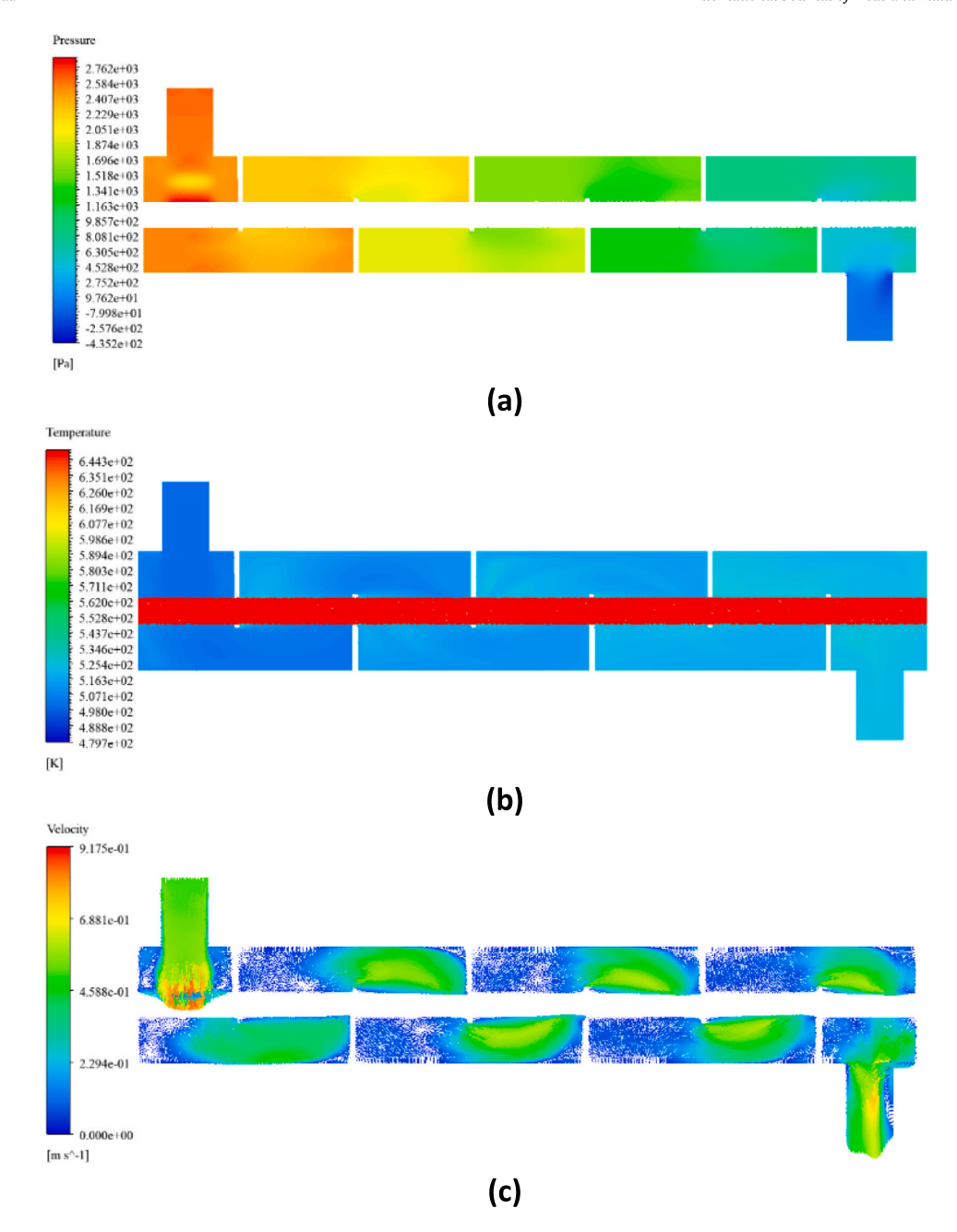


Fig. 17. (a) Pressure, (b) Temperature and (c) Velocity Contour of Solar Salt at 1.0 kg/s.

salts and mass flow rates. The 4 mm baffle holes also delivered impressive performance, with efficiency gains exceeding 15 %, while the 5 mm baffle holes achieved an average improvement of 30 %.

While the modified baffle design initially appears to reduce the system's heat transfer coefficient, it does not compromise efficiency. The design significantly reduces pressure drop, which outweighs the minor negative impact on heat transfer coefficient. This reduction allows the STHE to operate more efficiently, requiring less pumping power to manage the pressure drop, especially for high-viscosity fluids like molten salts used in this study. Often overlooked, pressure drop is a critical factor alongside heat transfer coefficient in optimizing system performance. In this case, the energy saved through lower pressure drop surpasses the small reduction in heat transfer coefficient. By analysing the performance index and overall system efficiency, the modified baffles prove to be a viable design choice for STHE applications, particularly in CSP systems utilizing molten salt as the heat transfer fluid.

3.7. Shell-side analysis of molten salts

To understand fluid behaviour within the shell-side of a heat exchanger, solar salt at a flow rate of 1.0 kg/s was selected as a representative case. This analysis is applicable to other molten salt in this study, albeit with varying values. Fig. 17(a) presents the pressure contour for solar salt, revealing the highest pressure at the shell inlet. As the fluid advances towards the outlet, a noticeable pressure drop occurs, particularly as it navigates through the baffles. This pressure reduction is attributed to the fluid's interaction with the baffles and walls, where it decelerates and, consequently, experiences a loss in pressure. The presence of baffles, while inducing a slowdown in fluid velocity, enhances heat exchange opportunities at the expense of increased pressure loss. Fig. 17 (b) delves deeper into this phenomenon, illustrating that significant heat exchange occurs near the walls and baffles, where fluid velocity is reduced.

Fig. 17 (c) velocity visualization further clarifies fluid movement.

Regions depicted in green indicate higher fluid velocities, which diminish upon collision with baffles, leading to turbulent zones, marked in blue, adjacent to the walls. These blue regions are critical for heat exchange due to the fluid's slowed velocity. This pattern of alternating high-velocity and turbulent zones persists from the heat exchanger's inlet to its outlet, optimizing the heat transfer process.

4. Conclusion

The CFD analysis indicated that NaKCaNO3 frequently outperformed the others, followed by Hitec, with solar salt trailing. At mass flow rates of 0.5 and 1.0 kg/s, Hitec led in achieving the highest shell outlet temperature, whereas NaKCaNO3 excelled at 2.0 kg/s. Conversely, solar salt consistently registered the lowest temperature values. In terms of pressure drop, Hitec experienced the most significant drop, closely followed by solar salt. NaKCaNO3 distinguished itself with the minimal pressure drop, although the variance between the molten salt with the highest and lowest pressure drop was modest, within a 5 % range. The overall heat transfer coefficient was least favourable for solar salt, with Hitec presenting improved values and NaKCaNO₃ topping the chart. The introduction of holes to the baffles resulted in a slight reduction in the fluid heat transfer coefficient but significantly reduced the pressure drop. The best performance index was obtained using baffles with 6 mm diameter holes, where the pressure drop reduction was around 42 %, while the heat transfer coefficient reduction was around 17 %. Further analysis revealed that the modified STHE design achieved an impressive efficiency improvement of up to 60 %. This enhancement is primarily attributed to a significant reduction in pressure drop, which lowers the pumping power required for operation. Although a lower pressure drop typically results in a reduction in heat transfer coefficient, in this case, the decrease was minimal, while the benefits from pressure drop reduction were substantial, culminating in remarkable efficiency gains. Exceptional performance at a prohibitive cost could undermine a material's viability and the system's feasibility. Evaluating between the modified and original baffle designs highlights that the modified baffle design is undoubtedly the superior choice for CSP applications using molten salt, delivering a balanced trade-off between heat transfer performance and pressure drop.

This study offers valuable insights into the heat transfer characteristics of molten salts while exploring innovative modifications to heat exchanger baffles that enhance system efficiency. These findings lay a solid foundation for advancing more efficient and sustainable concentrated solar power (CSP) systems, addressing critical challenges such as high-temperature heat transfer performance measurements. The research underscores the scarcity of material property data, highlighting the pressing need for comprehensive datasets to facilitate informed material selection for CSP applications. Moreover, this study serves as a baseline for heat transfer comparison with other materials, especially molten salts. Future research could focus on investigating various molten salt mixtures, delving deeper into their heat transfer properties, and expanding the comparative database to support advancements in CSP technology.

CRediT authorship contribution statement

M.A. Khaliquzzama: Writing – review & editing, Writing – original draft, Visualization, Validation, Software, Resources, Investigation, Formal analysis, Data curation, Conceptualization. S.U. Masuri: Writing – review & editing, Validation, Supervision, Software, Investigation, Formal analysis, Data curation, Conceptualization. R. Saidur: Writing – review & editing, Supervision, Resources, Formal analysis, Conceptualization. Abdul Aziz Hairuddin: Supervision, Investigation, Formal analysis, Conceptualization. Suraya Mohd Tahir: Supervision, Methodology, Data curation, Conceptualization. Norhazwani Abd Malek: Writing – review & editing, Validation, Software, Methodology, Investigation.

Declaration of Competing Interest

This work was supported by Universiti Putra Malaysia under the grant UPM/GP-IPB/2020/9688701.

Data availability

The authors do not have permission to share data.

References

- N. Aeronautics, T. Sun, The balance of power in the Earth-Sun system, (2005).

 Mike, W., 2009, Concentrating solar power global outlook 09 why renewable energy
- Mike, W., 2009. Concentrating solar power global outlook 09 why renewable energy is hot. Phys. Fluids 20, 22–40.
- Dudda, B., Shin, D., 2013. Effect of nanoparticle dispersion on specific heat capacity of a binary nitrate salt eutectic for concentrated solar power applications. Int. J. Therm. Sci. 69, 37–42. https://doi.org/10.1016/j.ijthermalsci.2013.02.003.
- Renewables 2020 Global Status Report, Renewables Global Status Report, 2020. http://www.ren21.net/resources/publications/.
- Pourasl, H.H., Vatankhah, R., Khojastehnezhad, V.M., 2023. Solar energy status in the world: a comprehensive review. Energy Rep. 10, 3474–3493. https://doi.org/ 10.1016/j.egyr.2023.10.022.
- Pelay, U., Luo, L., Fan, Y., Stitou, D., Rood, M., 2017. Thermal energy storage systems for concentrated solar power plants. Renew. Sustain. Energy Rev. 79, 82–100. https:// doi.org/10.1016/j.rser.2017.03.139.
- Hu, Y., He, Y., Zhang, Z., Wen, D., 2019. Enhanced heat capacity of binary nitrate eutectic salt-silica nanofluid for solar energy storage. Sol. Energy Mater. Sol. Cells 192, 94–102. https://doi.org/10.1016/j.solmat.2018.12.019.
- Han, D., Guene Lougou, B., Xu, Y., Shuai, Y., Huang, X., 2020. Thermal properties characterization of chloride salts/nanoparticles composite phase change material for high-temperature thermal energy storage. Appl. Energy 264, 114674. https://doi. org/10.1016/j.apenergy.2020.114674.
- Paikar, M., Hosseinzadeh, K., Kermani, J.R., Ganji, D.D., 2024. Hydrothermal assessment of a double-pass shell and tube heat exchanger in the presence of blade turbulators with different configurations. Int. J. Thermofluids 21, 100577. https://doi.org/ 10.1016/i.ijft.2024.100577.
- A.D. Jadhav, T.A. Koli, CFD Analysis of Shell and Tube Heat Exchanger to Study the Effect of Baffle Cut on the Pressure Drop, 2 (2014) 1–7.
- Ambekar, A.S., Sivakumar, R., Anantharaman, N., Vivekenandan, M., 2016. CFD simulation study of shell and tube heat exchangers with different baffle segment configurations. Appl. Therm. Eng. 108, 999–1007. https://doi.org/10.1016/j.applthermaleng.2016.08.013.
- Ben, M., Bessrour, J., Kallel, F., 2022. Numerical investigation of the flow dynamics and heat transfer in a rectangular shell-and-tube heat exchanger. Case Stud. Therm. Eng. 32. https://doi.org/10.1016/j.csite.2022.101873.
- You, Y., Fan, A., Huang, S., Liu, W., 2012. Numerical modeling and experimental validation of heat transfer and flow resistance on the shell side of a shell-and-tube heat exchanger with flower baffles. Int. J. Heat Mass Transf. 55, 7561–7569. https:// doi.org/10.1016/j.ijheatmasstransfer.2012.07.058.
- Wang, X., Zheng, N., Liu, Z., Liu, W., 2018. Numerical analysis and optimization study on shell-side performances of a shell and tube heat exchanger with staggered baffles. Int. J. Heat Mass Transf. 124, 247–259. https://doi.org/10.1016/j. ijheatmasstransfer.2018.03.081.
- Duan, Z., Shen, F., Cao, X., Zhang, J., 2016. Comprehensive effects of baffle configuration on the performance of heat exchanger with helical baffles. Nucl. Eng. Des. 300, 349–357. https://doi.org/10.1016/j.nucengdes.2016.02.010.
- Dong, C., Zhou, X.F., Dong, R., Zheng, Y.Q., Chen, Y.P., Hu, G.L., Xu, Y.S., Zhang, Z.G., Guo, W.W., 2017. An analysis of performance on trisection helical baffles heat exchangers with diverse inclination angles and baffle structures. Chem. Eng. Res. Des. 121, 421–430. https://doi.org/10.1016/j.cherd.2017.03.027.
- Shinde, S., Pancha, H., 2012. Comparative thermal performance analysis of segmental baffle heat exchanger with continuous helical baffle heat exchanger using Kern method, Mustansir hatim Pancha / int. J. Eng. Res. Appl. 2, 2264–2271 www.ijera.
- Tasouji Azar, R., Khalilarya, S., Jafarmadar, S., 2014. Tube bundle replacement for segmental and helical shell and tube heat exchangers: Experimental test and economic analysis. Appl. Therm. Eng. 62, 622–632. https://doi.org/10.1016/j. applthermaleng.2013.10.009.
- Awad, A., Navarro, H., Ding, Y., Wen, D., 2018. Thermal-physical properties of nanoparticle-seeded nitrate molten salts. Renew. Energy 120, 275–288. https://doi. org/10.1016/j.renene.2017.12.026.
- Kuchibhotla, A., Banerjee, D., Dhir, V., 2020. Forced convection heat transfer of molten salts: a review. Nucl. Eng. Des. 362, 110591. https://doi.org/10.1016/j. nucengdes.2020.110591.
- Singh, T., Hussien, M.A.A., Al-Ansari, T., Saoud, K., McKay, G., 2018. Critical review of solar thermal resources in GCC and application of nanofluids for development of efficient and cost effective CSP technologies. Renew. Sustain. Energy Rev. 91, 708–719. https://doi.org/10.1016/j.rser.2018.03.050.
- Ozden, E., Tari, I., 2010. Shell side CFD analysis of a small shell-and-tube heat exchanger. Energy Convers. Manag. 51, 1004–1014. https://doi.org/10.1016/j.enconman.2009.12.003.
- Cruz, P.A.D., Yamat, E.-J.-E., Nuqui, J.P.E., Soriano, A.N., 2022. Computational fluid dynamics (CFD) analysis of the heat transfer and fluid flow of copper (II) oxide-water

- nanofluid in a shell and tube heat exchanger. Digit. Chem. Eng. 3, 100014. https://doi.org/10.1016/j.dche.2022.100014.
- Li, N., Wang, Y., Liu, Q., Peng, H., 2022. Evaluation of thermal-physical properties of novel multicomponent molten nitrate salts for heat transfer and storage. Energies 15. https://doi.org/10.3390/en15186591.
- Bell, K.J., 1981. Delaware method for shell side design. In: Kakaç, S., Bergles, A., Mayinger, F. (Eds.), Heat Exch. Therm. Fundam. Des, Hemisphere, New York, pp. 581-618.
- Du, B.C., He, Y.L., Wang, K., Zhu, H.H., 2017. Convective heat transfer of molten salt in the shell-and-tube heat exchanger with segmental baffles. Int. J. Heat Mass Transf. 113, 456–465. https://doi.org/10.1016/j.ijheatmasstransfer.2017.05.075.
- J. Ji, Y. Lu, B. Shi, R. Gao, Q. Chen, Numerical research on vibration and heat transfer performance of a conical spiral elastic bundle heat exchanger with baffles, 232 (2023). https://doi.org/10.1016/j.applthermaleng.2023.121036.
- Taghizadeh-Tabari, Z., Zeinali Heris, S., Moradi, M., Kahani, M., 2016. The study on application of TiO2/water nanofluid in plate heat exchanger of milk pasteurization industries. Renew. Sustain. Energy Rev. 58, 1318–1326. https://doi.org/10.1016/j.rser.2015.12.292.